Restoring and sustaining human postmortem retinal light responses with scalable methods for testing degenerative disease therapies

Silke Becker[1,*], Jordan Allen[1,2,*], Zia L'Ecuyer Morison[1], Sama Saeid[3], Ari Koskelainen[3], Frans Vinberg[1,2,4 †].

*, co-first author, Silke Becker and Jordan Allen contributed equally.

[1] John A. Moran Eye Center, University of Utah, Salt Lake City, Utah, USA

[2] Department of Biomedical Engineering, University of Utah, Salt Lake City, Utah, USA

[3] Department of Neuroscience and Biomedical Engineering, Aalto University, Espoo, Finland

[4] Interdepartmental PhD Neuroscience Program, University of Utah, Salt Lake City, Utah, USA

[†] Corresponding author. John A. Moran Eye Center, University of Utah, Salt Lake City, Utah, USA. E-mail address: frans.vinberg@utah.edu

Science Advances

Neuro- and retinal degenerative diseases rob millions of aging individuals of their independence. Researching these diseases in human tissue has been hindered by the immediate loss of electric activity in neurons after the circulation ceases. Recent studies indicate that limited neuronal activity can be revived postmortem, even in the retina. We capitalized on this discovery by successfully restoring and maintaining *in vivo*-like light responses in eyes recovered up to four hours and stored for up to 48 hours postmortem. This breakthrough significantly increases the availability of functionally viable human retinas for research. Our AI-based postmortem retinal imaging platform identifies retinal structures and allows us to compare light responses in the healthy central and peripheral retina with *ex vivo* electroretinography. We use this platform to measure the dark adaptation of human macular cones from controls and donors with age-related macular degeneration for the first time in the absence of the retinal pigment epithelium. We developed increased throughput technology and a model to simulate disease-associated acute ischemia-reperfusion. In this model, we demonstrate the protective or toxic effects of several drugs targeting oxidative stress or glutamate excitotoxicity.

INTRODUCTION

Despite extensive animal research, more than 90 % of clinical trials for Investigational New Drugs (INDs) fail to progress to market approval [1], [2], often due to inadequate safety and efficacy data from animal models [3], [4], [5], [6], [7]. Particularly, small animal models or *in vitro* assays frequently struggle to replicate the complex pathologies of retinal diseases, e.g., age-related macular degeneration (AMD) and glaucoma, which involve advanced age, multiple genetic risk factors of low penetrance, and various environmental and lifestyle factors [3]. The retinas of non-human primates share many similarities with those of humans, but currently, retinal disease models in these species are limited to some forms of inherited retinal degeneration [8]. Additionally, ethical concerns and high costs limit the use of non-human primates [3]. Research in human postmortem eyes from donors with and without retinal diseases could overcome many of these obstacles and offer hope for new treatments for millions of patients who lose vision and quality of life.

Until recently, consensus decreed that neurons in the central nervous system, including the retina, rapidly and irreversibly deteriorate after the blood circulation ceases [9], [10], [11], [12]. Challenging this long-held belief, the pig brain can regain metabolic and spontaneous neuronal activity several hours after death, although synchronized global activity remains absent [13], [14]. We recently restored *in vivo*-like light responses, including synaptic transmission between retinal neurons, in postmortem human retinas from organ donor eyes recovered within 20 minutes of circulation loss [15]. Eyes enucleated 1-5 hours after death only exhibited photoreceptor responses but lacked postsynaptic ON-bipolar cell responses [15]. Inner retinal neurons can recover some of their spontaneous activity and light responsiveness depending on the duration of hypoxia or ischemia [16], [17], [18]. Shortages of functionally viable human eyes that preserve their inner retina ON-bipolar cell responses limit the usefulness of the postmortem human retina.

Studies on central retinal artery occlusion in rhesus monkeys indicate that retinal damage can be reversible depending on the duration of ischemia. Retinal light responses partially recovered several weeks after the circulation had been restored, even after three hours of retinal ischemia [17]. Efforts to preserve the brain have not exceeded six hours after the circulation was restored [13], [14], leaving the potential for a more complete recovery over a longer time unclear. In this study, after supplying the retina with sufficient nutrients and oxygen overnight, we routinely recorded *in vivo*-like light responses in human eyes collected 30-60 minutes postmortem from donors after brain or cardiac death (DBD and DCD), and in some cases even 3-4 hours after death. We sustained these light responses for at least 48 hours in intact human eyecups.

To enhance our technique's effectiveness, we introduce new *ex vivo* infrared OCT and fundus imaging technology to identify retinal structures. Our small-volume closed perfusion system, paired with a novel

eight-channel *ex vivo* electroretinography system, preserves photoreceptor light responses in isolated human neural retina samples for at least 12 hours, permitting the efficient use of this rare resource. Finally, we present a functional *ex vivo* assay to model diseases associated with acute ischemia-reperfusion injury, such as central retinal artery occlusion, which we used to test drugs that target ischemia-reperfusion injury. This demonstrates that our assay can be used for preclinical drug testing, with the potential to be expanded to AMD, diabetic retinopathy, glaucoma, retinal artery occlusion, and CNS conditions such as stroke.

By expanding access to and maximizing data output from functionally viable human retinas, our achievements will open new avenues for studying retinal diseases and streamline the successful progression of INDs into clinical trials. Our work also lays the foundation for testing novel gene therapies [19], [20], cell replacement therapies [21], and retinal prostheses [22] for patients with no other treatment options, as well as supporting recent efforts to restore vision through whole eye or retina transplantation [23].

RESULTS

Restoring and preserving light signaling in human donor retinas

We previously revived photoreceptor and ON-bipolar cell light responses when eyes were recovered within 20 minutes of circulatory arrest (cross-clamp). In contrast, we only recorded photoreceptor light responses if enucleation was delayed by more than one hour [15]. To explore the necessary time window for restoring light responses with *ex vivo* ERG, we partnered with the Utah Lions Eye Bank and the Organ Procurement Organization DonorConnect in Salt Lake City, Utah, to obtain whole human globes or posterior poles (after collection of the corneas for transplantation) from DBD and DCD cases.

Peripheral retinas from five DCD donors collected 50-60 minutes after circulatory arrest showed only small photoreceptor light responses during the first 1-2 hours after arriving in the laboratory (**Fig 1A**). Since ischemic damage can be reversed in models of central retinal artery occlusion [17], we tested whether overnight incubation could improve light responses. Indeed, by incubating eyecups (with the cornea, lens, and some of the vitreous removed) or pieces of the posterior eye in oxygenated bicarbonate-buffered Ames' media at room temperature overnight (**Fig 1B**), we revived postsynaptic ON-bipolar cell light responses (**Fig 1C, E, F**) and recorded large photoreceptor light responses (**Fig 1D**) in eyes collected within 50-60

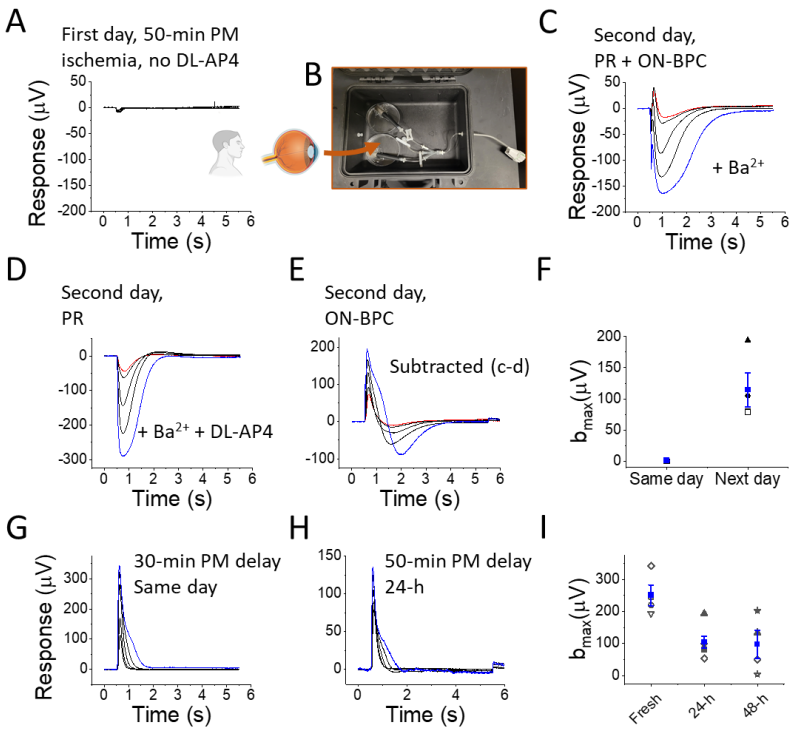

Figure 1. Restoring and preserving ERG b-waves in organ donor eyes after overnight eyecup incubation. (A) *Ex vivo* ERG light responses from the peripheral retina of an eye enucleated 50 min postmortem, recorded on the same day. In the absence of DL-AP4 only small a-waves were observed. (B) Overnight incubation of the eyecup in oxygenated media in darkness. (C) Light responses of a peripheral retina sample (after overnight eyecup incubation) in the presence of Ba^{2+} alone and (D) combined with DL-AP4. (E) Subtracting responses in (D) from those in (C) isolates a strong b-wave. (F) Maximum b-wave amplitudes (i.e., blue trace in (E) from three donors with 50-65-min enucleation delay, recorded ~3 h postmortem (Same day) or after overnight incubation (Next day) (Blue: mean ± SE). (G) *Ex vivo* ERG b-waves determined by subtraction, as shown in c-e, from human DBD eye enucleated within 30 min after death and recorded on the same day and (H) from human DCD eye enucleated within 50 min after death and recorded following 48 h incubation. (I) Maximal b-wave amplitudes (mean ± SE) from peripheral samples recorded soon after enucleation (fresh, 3 donors with <30 mins enucleation delay), 24 (5 donors with <60-mins enucleation delay) and 48 h (4 donors with <60-mins enucleation delay) after enucleation. Light flash strengths ranged from 19 to 1,014 photons (530 nm) μm^{-2}.

minutes. Notably, this protocol also restored ON-bipolar cell responses in 2 out of 5 pairs of research donor eyes enucleated 3-4 hours postmortem (**Supplementary Fig 1**).

It is crucial that the retina remains attached to the retinal pigment epithelium (RPE) during incubation. Isolated mouse retinas lost almost all of their ON-bipolar cell and much of their photoreceptor light responses during overnight incubation, even when kept in oxygenated media (**Supplementary Fig 2**). These findings show that postmortem ischemic injury can be reversed after prolonged incubation of retinas attached to the RPE, provided the eyes are enucleated and placed in oxygenated media within approximately one hour, or in some cases, several hours, from the loss of circulation.

Although human retinal organoids and, on occasion, neural retinas have been cultured long-term [11], [24], [25], [26], [27], [28], preservation of the whole human posterior eye *ex vivo* remains largely unexplored. To determine the duration for which retinal light responses can be maintained, we incubated posterior eyecups in oxygenated bicarbonate-buffered Ames' media at room temperature, as described above (**Fig 1B**). We punched 5 mm retina samples near the macula at 12-, 24-, and 48-hours postmortem and determined the subtracted *ex vivo* ERG b-wave amplitude (ON-bipolar cell response) as a sensitive biomarker for viability, as described in **Fig 1C-E.** With good retinal attachment and sterile incubation

media, we preserved ON-bipolar cell light responses for at least 48 hours (**Fig 1G-H**), although the maximum response amplitudes declined over time (**Fig 1I**).

Visualizing and Collecting Human Retina Samples for *Ex Vivo* ERG Recordings

The macula and fovea, located in the central retina and unique to humans and non-human primates among mammals, mediate high-acuity daytime color vision [29]. Current animal models fail to faithfully recapitulate the physiology and pathophysiology of the central retina, making it challenging to study diseases that affect high-acuity vision, e.g., in age-related macular degeneration [3]. Additionally, existing technologies do not permit studying macular physiology in postmortem eyes from healthy donors and patients with retinal diseases. To fill this gap, we adapted an existing imaging platform to enable precise sample collection from human donor eyes while preserving retinal light sensitivity.

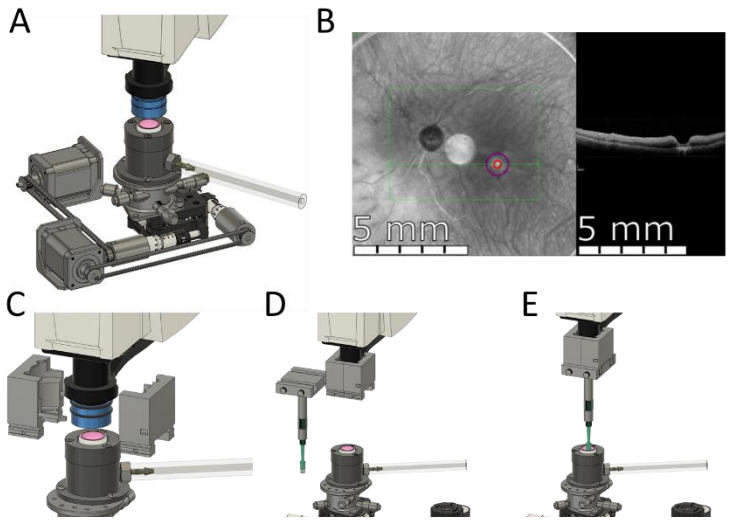

Figure 2. Foveal analysis and procurement automation. (A) Fundus and OCT imaging of *ex vivo* human eyecup. (B) Deep learning models scan the retina, locate the fovea and move the retina into position. (C-D) Biopsy punch attachment affixed to OCT lens. (E) Sampling of the fovea.

We adapted a Heidelberg Spectralis Optical Coherence Tomography (OCT) and fundus imaging platform for *ex vivo* analysis of eyecups under infrared light (**Fig 2A, B**). Typically used for high-resolution cross-sectional images of the retina in clinical settings, we adapted the OCT to image postmortem eyecups filled with Ames' media after the cornea and lens were removed to provide a clear optical path. A custom scanner lens adapter was created with Fusion 360, with which an additional lens was securely fitted to correct for altered refraction after removing the lens and cornea (shown in blue in **Fig 2A and C**; non-contact animal imaging lens, +25 Diopter, from Heidelberg Engineering Inc.). This setup allows us to image the retina and accurately locate the fovea in human donor eyes (**Fig 2B**).

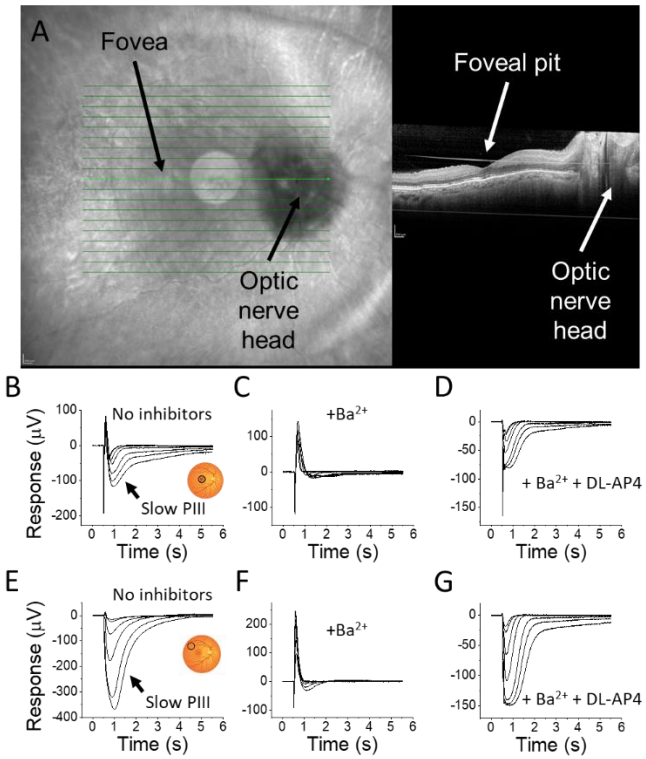

Figure 3. Imaging and recording of light responses from the central and peripheral human retina. (A) Infrared fundus and OCT image of the postmortem human retina from an eye enucleated 30 min postmortem. Retinal light responses in the central (B-D) and peripheral (E-G) retina from a DBD eye. Macular and peripheral light responses from the same eye shown in (A), (B, E) without inhibitors, (C, F) with 100 µM $BaCl_2$ to block glial responses and (D, G) with $BaCl_2$ and 40 µM DL-AP4 to remove glial and inner retina components. Light flash strengths at 530 nm wavelength ranged from 19 to 3,525 photons μm^{-2}.

An attached punch mechanism to collect retinal samples (**Fig. 2C-E**) (https://github.com/jordanallen291/Automatic-Foveal-Detection) achieved a puncture localization accuracy of 0.100 ± 0.066 mm across 24 trials (**Supplementary Fig 3A**). Although effective with a 100 % success rate (9/9) under illuminated conditions (**Supplementary Fig 4**), this method was prone to human error under dim red light in our electrophysiology suite, prompting us to develop two deep-learning models that automatically locate the fovea. The first model used a binary classification scheme to determine whether OCT images contain a fovea with 100% accuracy in the training and validation phases (**Supplementary Fig 3B**). The second model, based on the Ultralytics YOLO v8 architecture, precisely located the foveal coordinates with 98% precision and a 90% recall across images. This model effectively identified instances of the target class, 'fovea', in 30 validation images (**Supplementary Fig 3C**). All code and AI models are available on GitHub (https://github.com/jordanallen291/Automatic-Foveal-Detection).

Using the described fundus- and OCT-imaging, we collected the foveal pits and surrounding maculae (**Fig 3A**). Light responses from a DBD donor, who had been on life support for four days, showed strong photoreceptor and downstream retinal neuronal light responses in the central and peripheral retina regions (**Fig 3D, C and G, F**, respectively). Despite a 30-minute enucleation delay after cross-clamp, these responses resembled those with shorter 0-20 minute postmortem enucleation delays that we reported previously [15] and demonstrate successful recovery of robust light responses with extended postmortem delays.

In addition, we are the first to identify a Ba^{2+}-sensitive slow negative wave, known as the slow PIII (glial) component, in the macular region of the human retina (**Fig 3B**). The slow PIII wave has been

extensively described in cold-blooded species and rodents and likely arises from K^+ buffering by Müller glial cells [30], [31], [32], [33]. In the human peripheral retina, the slow PIII component was noticeably larger and similar to that in mice, compared to the smaller Ba^{2+}-sensitive component in the macula (**Fig 3B, E**).

Increasing the capacity of *ex vivo* ERG to test multiple human retina samples

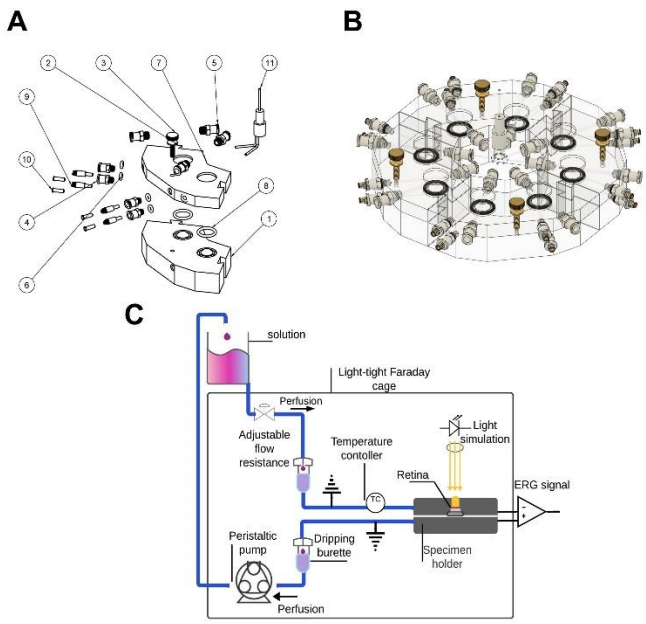

Figure 4. Multichannel specimen holder and closed-perfusion system to increase *ex vivo* ERG capacity. (A) Exploded view of eight-channel *ex vivo* ERG specimen holder with 1) Specimen holder bottom. 2) Specimen holder top. 3) Brass flared-collar knurled-head thumb screws. Electrodes made up of 4) Plastic quick-turn tube coupling, 6) Water-resistant neoprene O-ring, 9) Hot glue, 10) 2 mm socket. 5) Plastic quick-turn tube coupling to connect perfusion. 7) Water-resistant neoprene O-ring. 8) Oil-resistant hard buna-n O-ring. 11) MP-8 Manifold. (B) Assembled 8-channel *ex vivo* ERG specimen holder. (C) Schematic diagram of small-volume closed perfusion system and *ex vivo* ERG.

The size of the human eye allows us to collect multiple samples, enabling efficient electrophysiology recordings from a single retina. To maximize the use of this valuable tissue, we developed an eight-channel *ex vivo* ERG specimen holder, with each module containing a separate perfusion channel and electrodes for simultaneous experiments (**Fig 4A, B**). Mechanical drawings for CNC machining or 3D printing of this setup are available on GitHub (https://github.com/jordanallen291/Automatic-Foveal-Detection).

To create a drug testing platform that minimizes drug usage [34], we built a closed perfusion system that recirculates small perfusate volumes (150-180 mL) using a peristaltic pump, as shown in the simplified diagram in **Fig 4C**. After overnight incubation of three human donor eyecups with 1–4-hour enucleation delays, peripheral retina samples maintained stable *ex vivo* rod photoreceptor light responses for at least 12 hours after initiating perfusion in the *ex vivo* ERG specimen holder. During this time, the dim flash response time-to-peak and amplitude, the normalized amplitude to the maximal response, the maximum response, the normalized maximum response to the initial response, and the flash strength producing half-maximal responses remained stable (**Fig 5**).

Consistent results from all three donor retinas confirmed that our setup preserves retinal function during extended recordings with a minimal perfusate volume. This small-volume closed perfusion system integrates with the eight-channel *ex vivo* ERG platform we described earlier.

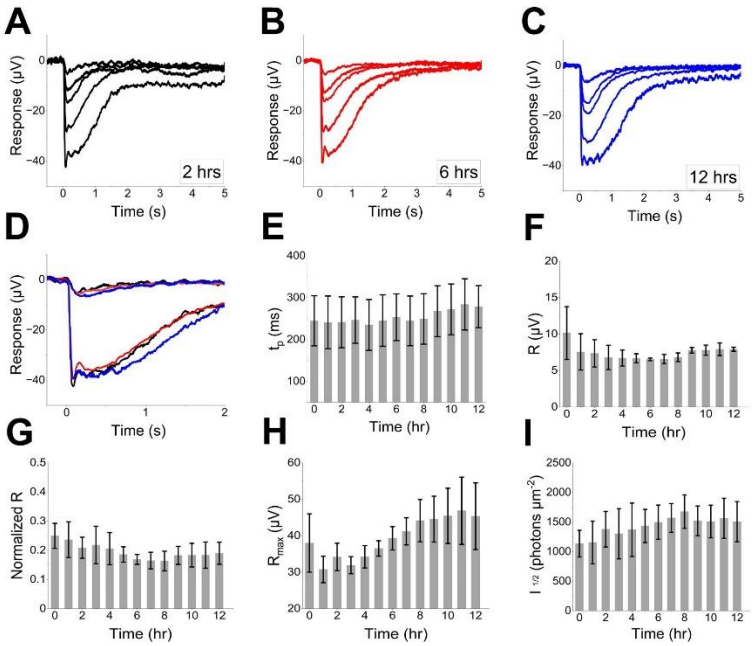

Figure 5. Preservation of ERG a-waves in the human retina during small-volume closed perfusion. (A-C) Example traces from a 38-year-old anoxic brain injury case with a one-hour post-mortem enucleation delay. (D) Preservation of dim and bright photoreceptors light responses at 2 (black), 6 (red) and 12 hours (blue) after perfusion was started. (E) time to peak, (F) dim stimulus amplitude (R), (G) normalized amplitude to the maximal response, (H) maximum response and (I) light sensitivity ($I_{1/2}$). Data in E-I is from three donors (UFT8, D54_2 and D55, see table 1), mean±SEM.

Drug Testing in the Human Retina and Development of an Ischemia-Reperfusion Injury Model

Several *in vivo* animal models study ischemia-reperfusion injury in the eye and brain caused by, e.g., cardiac arrest, stroke, and central retinal artery and vein occlusion [12], [17], [35], [36], [37], [38]. However, there are no existing *ex vivo* models to assess retinal function following ischemia-reperfusion injury in postmortem human retinas. To address this gap and expand the use of our *ex vivo* testing platform, we developed an acute ischemia-reperfusion injury model that replicates neuronal damage caused by hypoxia and reoxygenation.

In our model, we superfused isolated mouse retinas with hypoxic Ames' media (~2.5% O_2) while recording *ex vivo* ERG. We observed that ON-bipolar cells lost their light responses within several minutes, while photoreceptors retained >50% for at least 30 minutes (**Supplementary Fig 5**). This demonstrates that ON-bipolar cells are more vulnerable to hypoxia compared to photoreceptors.

We subsequently exposed mouse eyecups to low oxygen concentrations by immersing them in Ames' media directly bubbled with 0% O_2 for one or three hours. Immediately after hypoxia, light responses were substantially reduced, with a longer duration of hypoxia resulting in greater loss of light responses, particularly in ON-bipolar cells (**Fig 6A-C**). Overnight incubation in oxygenated Ames' media fully restored photoreceptor and ON-bipolar cell function after one hour of hypoxia, but only partially restored function after three hours of hypoxia (**Fig 6A-C**). In a human donor retina, three hours of hypoxia did not significantly decrease photoreceptor light responses but nearly eliminated ON-bipolar cell light responses, which mostly recovered during overnight incubation in oxygenated Ames' media (**Fig 6D-F**).

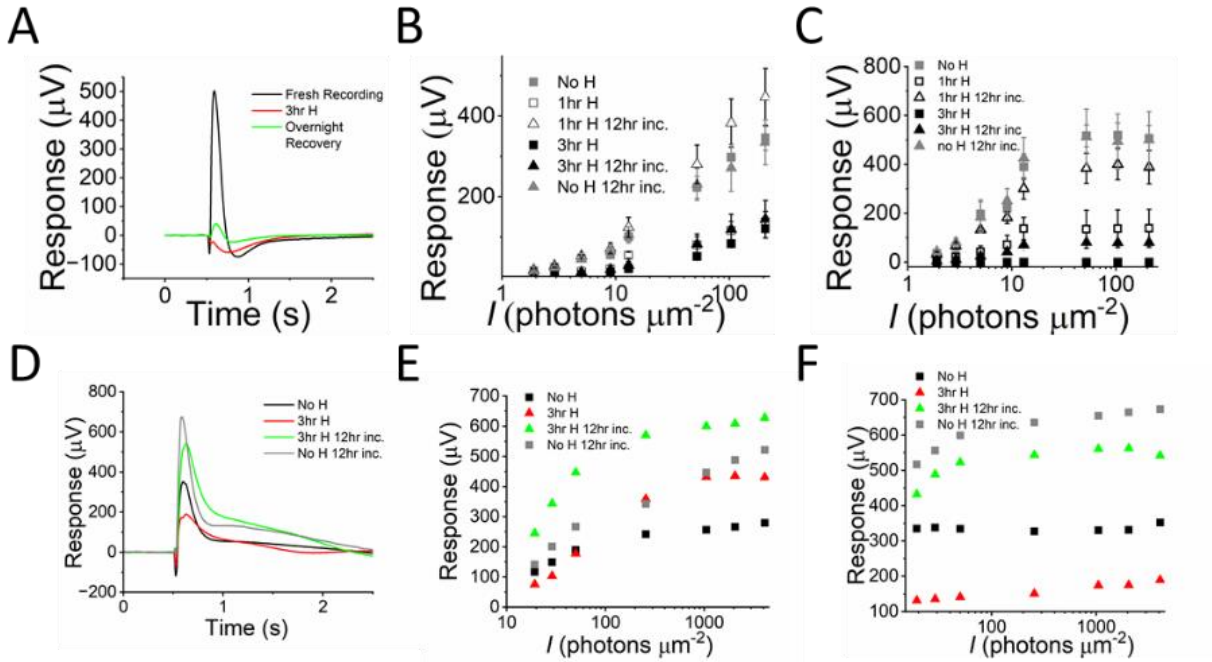

Figure 6. Ischemia-Reperfusion Injury Model in the Mouse and Human Retina. (A) Light responses before hypoxia (black), immediately after three hours of hypoxia (red), after overnight incubation without hypoxia (grey), and after three hours of hypoxia and overnight recovery in oxygenated media (green) in (A) mouse and (D) human retina. Averaged data summarizing effects of one or three hours of hypoxia with and without overnight recovery in oxygenated media compared to retinas kept in high oxygen, (B) in mouse (n=2-5) and (E) human photoreceptors (n=1) and (C) mouse (n=2-5) and (F) human ON-bipolar cells (n=1).

Hypoxia and ischemia-reperfusion injury cause cellular damage partly by increasing reactive oxygen species (ROS) production via the mitochondrial electron transport chain and NADPH oxidase [12], [39]. To counteract this we tested several pharmacological agents: Dimethyl malonate (DMM), a succinate dehydrogenase blocker, was used to prevent succinate accumulation during hypoxia and reduce ROS production in the mitochondrial electron transport chain during reoxygenation [40]. Apocynin blocks the assembly and production of ROS by NADPH oxidase [41]. While neither drug prevented the immediate loss of retinal light responses after one hour of hypoxia (**Fig 7A, B**), both apocynin and DMM improved overnight photoreceptor, but not ON-bipolar cell, recovery after three hours of hypoxia (**Fig 7C, D**). This implies that excessive production of ROS during reoxygenation impairs photoreceptor, but not ON-bipolar cell responses.

By carefully timing and combining these inhibitors we revealed some of the underlying repair mechanisms: DMM most effectively protected photoreceptors when administered during hypoxia or just before reoxygenation (**Supplementary Fig 6**), suggesting that succinate accumulation during hypoxia leads to a detrimental burst of ROS by reversing succinate dehydrogenase immediately upon reoxygenation. Applying DMM only during reoxygenation did not protect photoreceptor function (**Supplementary Fig 6**). Interestingly, combining DMM and apocynin was less protective for photoreceptors than apocynin alone,

while the general ROS scavenger α-lipoic acid impaired photoreceptor recovery (**Supplementary Fig 6**). These findings suggest that limited ROS production may be necessary to prevent or repair ischemia-reperfusion injury.

Since none of these pharmacological agents alone or in combination was protective for ON-bipolar cells (**Supplementary Fig 6**), excessive ROS production by the electron transport chain and the NADPH oxidase may not be the main mechanisms of damage to ON-bipolar cells, although ROS production may confer protection after hypoxia, similar to photoreceptors.

Finally, we tested two NMDA receptor blockers, MK-801 and memantine, to target potential glutamate excitotoxicity on photoreceptors and bipolar cells. Neither drug was protective, and MK-801 was detrimental to light responses after three hours of hypoxia (**Fig 8**).

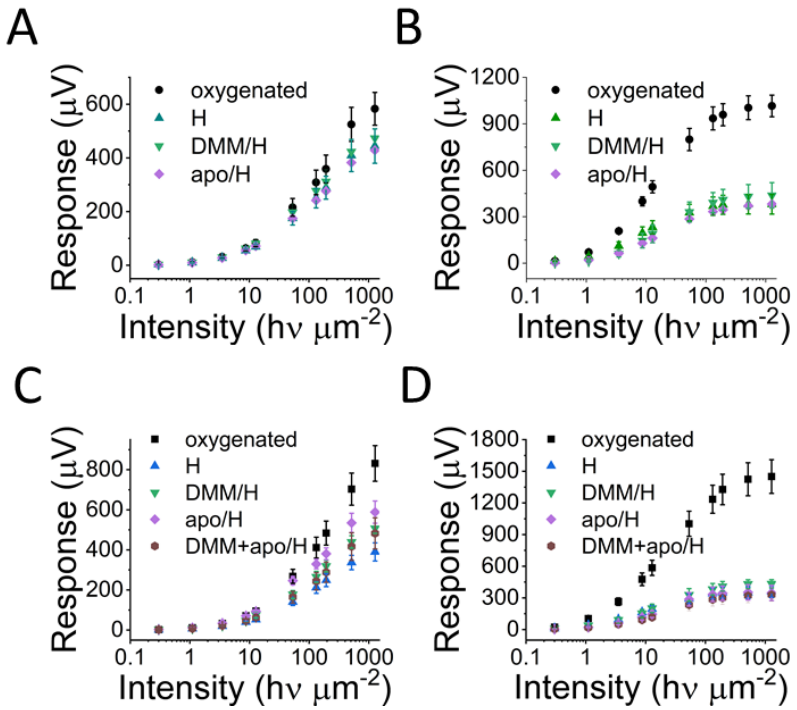

Figure 7. Preventing retinal injury during hypoxia and reoxygenation. Photoreceptor (A, C) and ON-bipolar cell light responses (B, D) in oxygenated media or (A, B) immediately after one hour of hypoxia or (C, D) after three hours of hypoxia with overnight incubation in oxygenated Ames' media in the absence or presence of dimethyl malonate (DMM) or apocynin (apo, n=4-6).

DISCUSSION

The retina originates from [42] and has long been considered a suitable model for the central nervous system [43]. Therefore, the functional human retina holds significant potential for studying the pathophysiology of neuronal diseases and testing INDs, including e.g., base editors as a new type of gene therapy for human inherited retinal diseases [19]. Thus far several limitations have restricted the usefulness of the postmortem human retina for large-scale physiological experiments, including the need for ultra-fresh human tissue, challenges to preserving light responses in the laboratory over time, difficulties in collecting retina samples from precise locations, and inability to use multiple retina samples simultaneously to maximize experimental output. We address these weaknesses in the present study: To scale up access to functionally viable human eyes, we worked with the Utah Lions Eye Bank and DonorConnect to establish the infrastructure and procedures for up to weekly recovery, transportation, and preservation of functionally

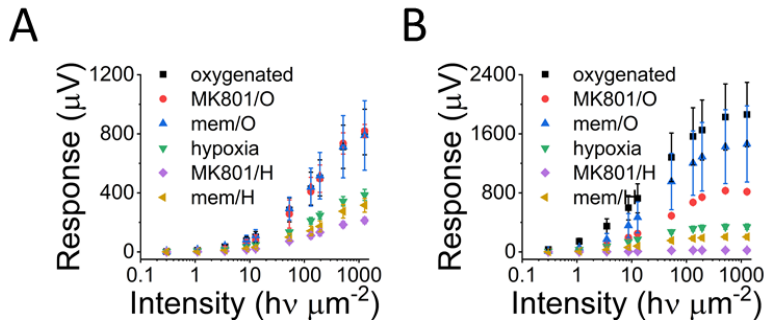

Figure 8. NMDA receptor blockers do not prevent retinal injury during hypoxia and reoxygenation. Photoreceptor (A) and ON-bipolar cell light responses (B) in oxygenated media (O) in the absence or presence of MK-801 or memantine or after three hours of hypoxia with overnight incubation in oxygenated Ames' media (H) in the absence or presence of MK-801 or memantine (mem, n=2-6).

viable human eyes from DBD and DCD cases (**Fig 1, 3**). This establishes a premise for studying physiology, network activity and computations of the human neurons in intact CNS tissue.

Our previously published data clearly showed that photoreceptors maintain their light responses more effectively during postmortem ischemia and better recover their function immediately after hypoxic injury compared to ON-bipolar cells, both in mice and in humans [15]. Here we report that, despite ON-bipolar cell light responses being exceedingly sensitive to hypoxia compared to photoreceptors (**Figure 7, Supplementary Fig 5**), we can restore light responses from peripheral ON-bipolar cells by overnight incubation of the mouse or human eyecups in oxygenated Ames' media even after 60 minutes of postmortem ischemia or hypoxia (**Fig 1, 7**). The same protocol sometimes, but not always, restores peripheral rod ON-bipolar cell responses and always improves photoreceptor response amplitudes in research donor eyes enucleated 3-4 hours postmortem, even though their responses remain smaller than those recorded from freshly recovered organ donor eyes (**Supplementary Fig 4**).

Our findings are consistent with a recent study that reported cellular recovery after 1-h warm ischemic time in pig brains [14]. These data imply that, instead of collectively undergoing hypoxia-induced apoptosis, at least a sizeable proportion of retinal neurons survive. Loss of ON-bipolar cell light responses must, therefore, be attributed to either temporary loss of synaptic connectivity between photoreceptors and ON-bipolar cells and/or ischemia-induced depolarization of ON-bipolar cells preventing light signal transmission in the inner retina. However, irrespective of the mechanism(s) underlying the transient loss of ON-bipolar cell function, we importantly not only extend access to functionally viable human eyes but also question whether ischemic or hypoxic retinal or brain injury is truly irreversible and can be repaired as long as cells remain preserved. Even though we consistently restored and preserved cone photoreceptor light responses in the maculae from DCD and research donors, and rod-mediated a- and b-waves in the peripheral retina, signal transmission to cone ON-bipolar cells remained elusive, indicating that the central retina and/or cone pathway may be more susceptible to ischemic injury. Our future research must, therefore, identify improved methods that consistently retain or restore ON-bipolar cell light responses in the central retina.

Removing the human retina from its physiological environment is both a limitation and a valuable tool of our method, enabling us to separate systemic from cell-intrinsic changes. *Ex vivo* ERG in human donor retinas also overcomes many disadvantages of alternative techniques: Age-related physiological changes are challenging to replicate in mice with their shorter lifespans or in retinal organoids, which largely follow the time course of retinal development [3], [11]. While transgenic mice may model monogenic inherited retinal degenerative diseases well, their genetic differences and lack of discernable phenotypes make them poor models of other mutations, such as many associated with age-related macular degeneration and glaucoma [3]. Central vision loss, a major cause of legal blindness, arises from cone degeneration, which cannot be studied in non-primate mammals. While non-human primates mirror many anatomical features of the human retina, including a macula, they lack in disease models and entail high costs and ethical concerns. By using human donor retinas, we maximize species-specific relevance of our findings, study aged retinas from donors with or without retinal diseases (**Fig 4**), and incorporate lifestyle and genetic factors that modulate retinal disease, all while reducing animal use and costs in vision research.

To support these goals, our study provides protocols and new technologies for long-term functional preservation, precise sample collection, high-throughput measurements, and disease phenotyping (**Fig 1-6**). These methods were further used to develop an ischemia-reperfusion assay for drug testing in *ex vivo* mouse and human retina (**Fig 7, 8**). Based on our previous findings that hypoxia is the likely cause of irreversible damage [15], we focused on hypoxia and reoxygenation, which, on the timescale of our *ex vivo* experiments matches, models acute conditions like central retina artery occlusion (CRAO) and stroke. Although our *ex vivo* approach does not fully capture chronic, low-grade ischemia seen in, e.g., AMD, glaucoma and diabetic retinopathy, future studies could include inflammation assays and comparisons of drug performance between clinical trials and our *ex vivo* system. Our platform bridges *in vitro* experiments in cell lines and *in vivo* animal testing, providing human tissue-relevant functional biomarkers that may correlate with clinically meaningful vision outcomes – something that is not feasible with *in vitro* approaches alone.

We initially targeted ischemia-reperfusion injury pathways focused on oxidative stress (**Fig 7, Supp Fig 6**) and glutamate excitotoxicity (**Fig 8**). These experiments showed that inhibiting specific ROS producing pathways, such as succinate dehydrogenase (Complex II) and NADPH oxidase, during and after hypoxia protected photoreceptor function. However, combining DMM and apocynin (inhibitors of Complex II and NADPH oxidase, respectively) proved less protective than apocynin alone, and broad-spectrum scavenging of ROS with α-lipoic acid was toxic. These results suggest that limited ROS may have protective effects against ischemia-reperfusion injury, whereas excess ROS are harmful, which future dose-

response studies with α-lipoic acid could test. Alternatively, targeting specific ROS-producing pathways may address distinct injury mechanisms that affect different neuronal compartments [44].

Interestingly, although DMM and apocynin preserved photoreceptor function, they did not protect bipolar cells, and drugs blocking glutamate excitotoxicity failed to preserve photoreceptors or ON-bipolar cells. Thes findings indicate that each retinal cell type may require different protective strategies, highlighting the need to develop drug combinations that protect all important retinal cell types without toxic effects.

Our methods promise to revolutionize research human retinal physiology and pathophysiology, with broader implications beyond ophthalmology. Insights from our retinal ischemia-reperfusion injury model may inform treatments for similar injuries in the CNS, including acute damage following ischemic stroke or brain injury after cardiac arrest, and chronic hypoxic diseases such as Alzheimer's and Parkinson's diseases, as well as age-related macular degeneration. Our platform will also facilitate preclinical testing of INDs for these conditions.

Furthermore, our work will support efforts to replace retinas or even whole eyes, similar to the pioneering whole-eye transplantation recently performed at NYU Langone Health [45] and an the audacious program announced by the US Department of Health to restore vision in bilaterally blind patients through whole-eye transplantation (THEA) [23], for which our work will provide a basis for novel techniques to recovering, reviving, and preserving light responses in the central and peripheral human retina function from DBD and DCD donors.

Acknowledgements

We thank Austin Adderley, Lana Gale, Marco Medina, and the recovery technicians at the Utah Lion's Eye Bank, Brent Davis and the Donor Connect Surgical Recovery Coordinators team, as well as the University of Utah and Intermountain transplant surgeons for their support in procuring human donor eyes. This work was supported by NEI R01 EY031706 to F. V., a DRC Research grant to S. B., National Institutes of Health Core Grant (EY014800), and an Unrestricted Grant from Research to Prevent Blindness, New York, NY, to the Department of Ophthalmology & Visual Sciences, University of Utah. Also, Dr. Frans Vinberg is a recipient of a Research to Prevent Blindness Dr. H. James and Carole Free Career Development Award. This work was also supported in part by the John A. Moran Eye Center (JMEC CORE) under Grant P30 EY014800 and Vision Research Training Grant T32 EY024234.

Bibliography

[1] D. Sun, W. Gao, H. Hu, and S. Zhou, "Why 90% of clinical drug development fails and how to improve it?," *Acta Pharm Sin B*, vol. 12, no. 7, pp. 3049–3062, Jul. 2022, doi: 10.1016/j.apsb.2022.02.002.

[2] A. Loewa, J. J. Feng, and S. Hedtrich, "Human disease models in drug development," *Nat Rev Bioeng*, vol. 1, no. 8, Art. no. 8, Aug. 2023, doi: 10.1038/s44222-023-00063-3.

[3] S. Becker, Z. L'Ecuyer, B. W. Jones, M. A. Zouache, F. S. McDonnell, and F. Vinberg, "Modeling complex age-related eye disease," *Prog Retin Eye Res*, vol. 100, p. 101247, May 2024, doi: 10.1016/j.preteyeres.2024.101247.

[4] A. Akhtar, S. M. Gupta, S. Dwivedi, D. Kumar, Mohd. F. Shaikh, and A. Negi, "Preclinical Models for Alzheimer's Disease: Past, Present, and Future Approaches," *ACS Omega*, vol. 7, no. 51, pp. 47504–47517, Dec. 2022, doi: 10.1021/acsomega.2c05609.

[5] T. M. Dawson, T. E. Golde, and C. L. Tourenne, "Animal Models of Neurodegenerative Diseases," *Nat Neurosci*, vol. 21, no. 10, pp. 1370–1379, Oct. 2018, doi: 10.1038/s41593-018-0236-8.

[6] S. Schnichels *et al.*, "Retina in a dish: Cell cultures, retinal explants and animal models for common diseases of the retina," *Progress in Retinal and Eye Research*, vol. 81, p. 100880, Mar. 2021, doi: 10.1016/j.preteyeres.2020.100880.

[7] J. Rivera and L. Tessarollo, "Genetic background and the dilemma of translating mouse studies to humans," *Immunity*, vol. 28, no. 1, pp. 1–4, Jan. 2008, doi: 10.1016/j.immuni.2007.12.008.

[8] D. Ail *et al.*, "Inducible nonhuman primate models of retinal degeneration for testing end-stage therapies," *Sci Adv*, vol. 9, no. 31, p. eadg8163, Aug. 2023, doi: 10.1126/sciadv.adg8163.

[9] J. Borjigin *et al.*, "Surge of neurophysiological coherence and connectivity in the dying brain," *Proc Natl Acad Sci U S A*, vol. 110, no. 35, pp. 14432–14437, Aug. 2013, doi: 10.1073/pnas.1308285110.

[10] S. L. Cole and E. Corday, "Four-minute limit for cardiac resuscitation," *J Am Med Assoc*, vol. 161, no. 15, pp. 1454–1458, Aug. 1956, doi: 10.1001/jama.1956.02970150022005.

[11] C. S. Cowan *et al.*, "Cell Types of the Human Retina and Its Organoids at Single-Cell Resolution," *Cell*, vol. 182, no. 6, pp. 1623-1640.e34, Sep. 2020, doi: 10.1016/j.cell.2020.08.013.

[12] N. N. Osborne, R. J. Casson, J. P. M. Wood, G. Chidlow, M. Graham, and J. Melena, "Retinal ischemia: mechanisms of damage and potential therapeutic strategies," *Prog Retin Eye Res*, vol. 23, no. 1, pp. 91–147, Jan. 2004, doi: 10.1016/j.preteyeres.2003.12.001.

[13] Z. Vrselja *et al.*, "Restoration of brain circulation and cellular functions hours post-mortem," *Nature*, vol. 568, no. 7752, pp. 336–343, Apr. 2019, doi: 10.1038/s41586-019-1099-1.

[14] D. Andrijevic *et al.*, "Cellular recovery after prolonged warm ischaemia of the whole body," *Nature*, vol. 608, no. 7922, pp. 405–412, Aug. 2022, doi: 10.1038/s41586-022-05016-1.

[15] F. Abbas *et al.*, "Revival of light signalling in the postmortem mouse and human retina," *Nature*, vol. 606, no. 7913, Art. no. 7913, Jun. 2022, doi: 10.1038/s41586-022-04709-x.

[16] C. Ingensiep, K. Schaffrath, B. Denecke, P. Walter, and S. Johnen, "A multielectrode array-based hypoxia model for the analysis of electrical activity in murine retinae," *J Neurosci Res*, vol. 99, no. 9, pp. 2172–2187, Sep. 2021, doi: 10.1002/jnr.24899.

[17] S. S. Hayreh, M. B. Zimmerman, A. Kimura, and A. Sanon, "Central retinal artery occlusion. Retinal survival time," *Exp Eye Res*, vol. 78, no. 3, pp. 723–736, Mar. 2004, doi: 10.1016/s0014-4835(03)00214-8.

[18] K. Reinhard *et al.*, "Hypothermia Promotes Survival of Ischemic Retinal Ganglion Cells," *Invest Ophthalmol Vis Sci*, vol. 57, no. 2, pp. 658–663, Feb. 2016, doi: 10.1167/iovs.15-17751.

[19] S. Suh *et al.*, "Restoration of visual function in adult mice with an inherited retinal disease via adenine base editing," *Nat Biomed Eng*, vol. 5, no. 2, pp. 169–178, Feb. 2021, doi: 10.1038/s41551-020-00632-6.

[20] M. Herrera-Barrera *et al.*, “Peptide-guided lipid nanoparticles deliver mRNA to the neural retina of rodents and nonhuman primates,” *Sci Adv*, vol. 9, no. 2, p. eadd4623, Jan. 2023, doi: 10.1126/sciadv.add4623.
[21] R. Sharma *et al.*, “Clinical-grade stem cell-derived retinal pigment epithelium patch rescues retinal degeneration in rodents and pigs,” *Sci Transl Med*, vol. 11, no. 475, p. eaat5580, Jan. 2019, doi: 10.1126/scitranslmed.aat5580.
[22] Y. Hou *et al.*, “Retina-inspired narrowband perovskite sensor array for panchromatic imaging,” *Sci Adv*, vol. 9, no. 15, p. eade2338, Apr. 2023, doi: 10.1126/sciadv.ade2338.
[23] “THEA | ARPA-H.” Accessed: May 25, 2024. [Online]. Available: https://arpa-h.gov/research-and-funding/programs/thea
[24] X. Zhong *et al.*, “Generation of three-dimensional retinal tissue with functional photoreceptors from human iPSCs,” *Nat Commun*, vol. 5, p. 4047, Jun. 2014, doi: 10.1038/ncomms5047.
[25] K. C. Eldred *et al.*, “Thyroid hormone signaling specifies cone subtypes in human retinal organoids,” *Science*, vol. 362, no. 6411, p. eaau6348, Oct. 2018, doi: 10.1126/science.aau6348.
[26] Y. C. Leong, V. Di Foggia, H. Pramod, M. Bitner-Glindzicz, A. Patel, and J. C. Sowden, “Molecular pathology of Usher 1B patient-derived retinal organoids at single cell resolution,” *Stem Cell Reports*, vol. 17, no. 11, pp. 2421–2437, Nov. 2022, doi: 10.1016/j.stemcr.2022.09.006.
[27] V. Busskamp *et al.*, “Genetic reactivation of cone photoreceptors restores visual responses in retinitis pigmentosa,” *Science*, vol. 329, no. 5990, pp. 413–417, Jul. 2010, doi: 10.1126/science.1190897.
[28] A. Saha, E. Capowski, M. A. Fernandez Zepeda, E. C. Nelson, D. M. Gamm, and R. Sinha, “Cone photoreceptors in human stem cell-derived retinal organoids demonstrate intrinsic light responses that mimic those of primate fovea,” *Cell Stem Cell*, vol. 29, no. 3, pp. 460-471.e3, Mar. 2022, doi: 10.1016/j.stem.2022.01.002.
[29] H. Kolb, R. F. Nelson, P. K. Ahnelt, I. Ortuño-Lizarán, and N. Cuenca, “The Architecture of the Human Fovea,” in *Webvision: The Organization of the Retina and Visual System*, H. Kolb, E. Fernandez, and R. Nelson, Eds., Salt Lake City (UT): University of Utah Health Sciences Center, 1995. Accessed: Jun. 03, 2024. [Online]. Available: http://www.ncbi.nlm.nih.gov/books/NBK554706/
[30] P. Witkovsky, F. E. Dudek, and H. Ripps, “Slow PIII component of the carp electroretinogram,” *J Gen Physiol*, vol. 65, no. 2, pp. 119–134, Feb. 1975, doi: 10.1085/jgp.65.2.119.
[31] D. A. Bolnick, A. E. Walter, and A. J. Sillman, “Barium suppresses slow PIII in perfused bullfrog retina,” *Vision Res*, vol. 19, no. 10, pp. 1117–1119, 1979, doi: 10.1016/0042-6989(79)90006-3.
[32] S. Nymark, H. Heikkinen, C. Haldin, K. Donner, and A. Koskelainen, “Light responses and light adaptation in rat retinal rods at different temperatures,” *J Physiol*, vol. 567, no. Pt 3, pp. 923–938, Sep. 2005, doi: 10.1113/jphysiol.2005.090662.
[33] P. Kofuji, P. Ceelen, K. R. Zahs, L. W. Surbeck, H. A. Lester, and E. A. Newman, “Genetic inactivation of an inwardly rectifying potassium channel (Kir4.1 subunit) in mice: phenotypic impact in retina,” *J Neurosci*, vol. 20, no. 15, pp. 5733–5740, Aug. 2000, doi: 10.1523/JNEUROSCI.20-15-05733.2000.
[34] L. Cangiano and S. Asteriti, “An Ex Vivo Electroretinographic Apparatus for the mL-Scale Testing of Drugs to One Day and Beyond,” *Int J Mol Sci*, vol. 24, no. 14, p. 11346, Jul. 2023, doi: 10.3390/ijms241411346.
[35] J. D. Sokolowski *et al.*, “Preclinical models of middle cerebral artery occlusion: new imaging approaches to a classic technique,” *Front Neurol*, vol. 14, p. 1170675, 2023, doi: 10.3389/fneur.2023.1170675.
[36] M. Renner *et al.*, “Optic Nerve Degeneration after Retinal Ischemia/Reperfusion in a Rodent Model,” *Front Cell Neurosci*, vol. 11, p. 254, 2017, doi: 10.3389/fncel.2017.00254.
[37] S. Evans *et al.*, “Ischemia reperfusion injury provokes adverse left ventricular remodeling in dysferlin-deficient hearts through a pathway that involves TIRAP dependent signaling,” *Sci Rep*, vol. 10, no. 1, p. 14129, Aug. 2020, doi: 10.1038/s41598-020-71079-7.

[38] N. Vestergaard, L. J. Cehofski, B. Honoré, K. Aasbjerg, and H. Vorum, "Animal Models Used to Simulate Retinal Artery Occlusion: A Comprehensive Review," *Transl Vis Sci Technol*, vol. 8, no. 4, p. 23, Jul. 2019, doi: 10.1167/tvst.8.4.23.
[39] D. N. Granger and P. R. Kvietys, "Reperfusion injury and reactive oxygen species: The evolution of a concept," *Redox Biol*, vol. 6, pp. 524–551, Dec. 2015, doi: 10.1016/j.redox.2015.08.020.
[40] E. T. Chouchani *et al.*, "Ischaemic accumulation of succinate controls reperfusion injury through mitochondrial ROS," *Nature*, vol. 515, no. 7527, pp. 431–435, Nov. 2014, doi: 10.1038/nature13909.
[41] J. Stefanska and R. Pawliczak, "Apocynin: Molecular Aptitudes," *Mediators of Inflammation*, vol. 2008, p. 106507, Dec. 2008, doi: 10.1155/2008/106507.
[42] D. Purves *et al.*, "The Retina," in *Neuroscience. 2nd edition*, Sinauer Associates, 2001. Accessed: Jul. 09, 2024. [Online]. Available: https://www.ncbi.nlm.nih.gov/books/NBK10885/
[43] A. Ames and F. B. Nesbett, "In vitro retina as an experimental model of the central nervous system," *J Neurochem*, vol. 37, no. 4, pp. 867–877, Oct. 1981, doi: 10.1111/j.1471-4159.1981.tb04473.x.
[44] A. Y. Abramov, A. Scorziello, and M. R. Duchen, "Three Distinct Mechanisms Generate Oxygen Free Radicals in Neurons and Contribute to Cell Death during Anoxia and Reoxygenation," *The Journal of Neuroscience*, vol. 27, no. 5, p. 1129, Jan. 2007, doi: 10.1523/JNEUROSCI.4468-06.2007.
[45] "NYU Langone Health Performs World's First Whole-Eye & Partial-Face Transplant," NYU Langone News. Accessed: May 12, 2024. [Online]. Available: https://nyulangone.org/news/nyu-langone-health-performs-worlds-first-whole-eye-partial-face-transplant
[46] R. N. Frank and J. E. Dowling, "Rhodopsin photoproducts: effects on electroretinogram sensitivity in isolated perfused rat retina," *Science*, vol. 161, no. 3840, pp. 487–489, Aug. 1968, doi: 10.1126/science.161.3840.487.
[47] F. Abbas, F. Vinberg, and S. Becker, "Optimizing the Setup and Conditions for Ex Vivo Electroretinogram to Study Retina Function in Small and Large Eyes," *J Vis Exp*, no. 184, Jun. 2022, doi: 10.3791/62763.
[48] F. Vinberg and V. Kefalov, "Simultaneous ex vivo functional testing of two retinas by in vivo electroretinogram system," *J Vis Exp*, no. 99, p. e52855, May 2015, doi: 10.3791/52855.

Methods

Donor Demographics, Eye Procurement and Transportation

Human eye tissue was procured by the Utah Lion's Eye Bank (Food and Drug Administration accreditation number 3000215349) in conjunction with whole organ donation by Donor Connect (Food and Drug Administration accreditation number 3000215350, Centers for Medicare & Medicaid Services accreditation number 46P001). The Utah Lion's Eye Bank obtained consent for research use for all donor eyes according to the Uniform Anatomical Gift Act (UAGA). The research team did not identify or select potential organ donors and had no access to non-anonymized donor information, except for information on ocular diseases, such as age-related macular degeneration and diabetic retinopathy. Our research project was, therefore, classified as exempt by the University of Utah (IRB no. 00106658).

Whole eyes or posterior poles were enucleated within 30-60 minutes after cross-clamp and transported to the laboratory in HEPES-buffered Ames' media that was directly bubbled with 100% O_2 at room temperature in the custom transportation case we previously described [15].

Eyes from research donors were enucleated up to 5 hours postmortem by a trained Eye Bank technician and immediately placed into HEPES-buffered Ames' media at room temperature. Eyes from organ donors were obtained up to 1 hour after cross-clamp at the time of organ removal, either with or without corneas, if these were transplanted, and placed into HEPES-buffered Ames' media and oxygenated with 100 % medical oxygen in our custom transportation case. From the time of retrieval, eyes were protected from light, stored at room temperature, and immediately transferred to the laboratory. Table 1 lists basic non-identifying information: age, sex, cause of death, cross-clamp/death-to-preservation delay, and potentially relevant medical conditions of all organ and research donors used in this study.

Sample Preparation

Upon arrival in the laboratory, eyes were handled under dim red-light illumination and stored in bicarbonate-buffered Ames' media oxygenated with 95 % O_2 and 5 % CO_2. By making an incision approximately 3-5 mm behind the limbus, we removed the anterior section of the eye with the lens, if applicable, and removed most of the vitreous to image the retina.

Hardware

OCT Adaptation and Sample Acquisition

We vertically reoriented an optical coherence tomography (OCT) machine (Spectralis, Heidelberg Engineering, Franklin, MA) to ensure that dissected eyecups would remain in place during imaging and

sampling. With Fusion 360 (Autodesk, San Rafael, CA), we machined an adapter plate from 6061 aluminum and secured the OCT scanner to additional mounting equipment (ThorLabs, Newton, NJ) uprightly. This and all other custom-made models and mechanical drawings are available on GitHub (https://github.com/jordanallen291/Automatic-Foveal-Detection).

We secured the eyecup in a custom-made vacuum chamber, which we had modeled in Fusion 360 and machined in 6061 aluminum. When we applied pressure of 1.773×10^4 Pa to porcine eyecups, they remained firmly in position with no discernable signs of external stress. Our custom fixture stage included a LX20/M translational state (X ±25 mm, Y ±25 mm), VAP4/M vertical translation stage (Z ±101.6 mm) and TTR001/M tip, tilt and rotational stage (roll α ±5°, pitch β ±5°, yaw γ ±10°, Thorlabs, Newton, NJ), which provided six degrees of freedom to position the eyecup precisely. After locating the fovea with OCT, we punched a 5 mm retina sample with a disposable biopsy punch (Fisher Scientific, Hampton, NH) on a 3D-printed lens attachment. Elastic O-rings (McMaster-Carr, Elmhurst, IL) reliably and safely secured the sliding biopsy mechanism to the OCT lens.

Positional Accuracy Validation

To validate the precision of the punch attachment, we marked twenty-four circles (~3 mm in diameter) as targets onto an affixed sticky note (3M, St. Paul, MN). A needle puncture outside the targets was marked with tape as the "reference area" before each target was translated to this location and punctured. The distance from the center of each hole to the target was recorded and reported as the mean difference and standard deviation. We used porcine eyecups to test the system's ability to excise retina samples accurately. To prepare the eyes for testing, we made a small incision near the limbus, submerged the eyes overnight in 4% paraformaldehyde in phosphate-buffered saline, and removed the anterior segment and most of the vitreous.

Using a 2 mm disposable biopsy punch, we made a minor impression in the retina to serve as a reference marker, whose location we marked on the OCT display to compensate for the offset between the OCT's optical axis and the axis of the biopsy punch. We then aligned the target area with the calibration marker and penetrated the eyecup with the biopsy punch to the sclera. The procedure was deemed successful if the target was accurately incised. This process was repeated three times in three different eyes, resulting in nine data points (N=9).

Software

We combined several Python scripts to automatically collect retinal images and apply deep learning models that classify images and detect objects. The main program, auto_sample.py, relies on capture_coordinates.py, ImgClassrevised.py, train_obj_det.py, and test_obj_det.py scripts.

Screen Coordinate Capture

In the automated workflow of auto_sample.py, the capture_coordinates.py script allows the precise capture of spatial data to interact with the OCT software by interactively collecting screen coordinates and color information through mouse clicks. These coordinates detect when the OCT software is ready for image acquisition and execute a sequence of mouse clicks that will save the acquired images for further analysis. Upon execution, the user is prompted to specify the number of coordinates to be saved. By utilizing both pyautogui and pynput.mouse libraries, the program listens for mouse click events. For each click, it captures and stores the corresponding screen location and the color at that point, leveraging pyautogui.screenshot().getpixel() to obtain the color information. This process documents the selected regions, allowing for automated mouse movement in auto_sample.py.

Image Classification

We trained the classification model in auto_sample.py using ImgClassRevised.py to sort OCT images into two categories, either with or without a fovea. The script initially sets up the environment and imports necessary libraries, including TensorFlow, to build and train the neural network and OpenCV for image manipulation. TensorFlow's image_dataset_from_directory function loads and labels 'fovea' and 'no fovea' images from predefined directories based on their folder structure, resizes the images to reduce the computational power needed to train the model, and places the images into batches of 32. The classification model was trained on 592 OCT images from human donor eyes that we had acquired under the same protocol before AI integration, evenly split between ‘fovea’ or ‘no fovea’ categories.

Most of the script preprocesses images by applying random brightness, contrast, saturation, and hue adjustments to optimize the model. The model’s architecture is constructed using TensorFlow's Keras API, starting with a convolutional base comprising four convolutional blocks, each followed by max pooling to distill features from OCT images efficiently. The initial block introduces 32 3x3 filters with ReLU activation, progressively increasing the filter count to 64 in the second, 128 in the third, and 256 in the fourth to capture a wide array of image features. After flattening the output to a single dimension, the model integrates two dense layers with 512 and 256 neurons, respectively, employing ReLU activation to process the features further. In the final step, a single neuron with a sigmoid activation function designed for binary classification discerns images from those with or without a fovea.

The dataset was divided into training, validation, and test sets to evaluate the model's performance accurately. Callbacks in the script save the best-performing model with the highest validation accuracy and log training progress, thus facilitating model tuning and evaluation. After training, the script plots loss and accuracy metrics over 30 epochs to visualize the learning process. Finally, users can save the trained model for future use.

Object Detection

The train_obj_det.py script delineates the training process of our object detection model and allows auto_sample.py to detect the location of the fovea in classified OCT images with the latest YOLOv8 architecture. The script employs the Ultralytics YOLO library to train a new YOLO model based on a predefined configuration file (yolov8n.yaml), which points to a separate training dataset of 261 annotated foveal images, collected as before with the ImgClassRevised.py script. The train_obj_det.py script ensures the use of GPU if available for faster processing. Its core function, locate_fovea, takes an image path and the YOLO model as inputs and runs inference on the image to predict the presence of a fovea and plots and displays its location. A matplotlib library visualizes the results and uses the PIL library for image processing. After training over 30 epochs, the script validates the model's performance using a separate set of 30 foveal images.

Automatic Sampling

With the data and models from the other scripts, auto_sample.py automatically locates and samples the foveal region of the retina. It initially monitors a predefined screen region to match a target color, indicating that the operator has obtained several b-scans of the retina, and saves the images from the OCT software. The images are each assigned a unique identification number to avoid overwriting existing data, which enables easy access for subsequent processing. The pre-trained script iterates through the saved images, applies necessary preprocessing, and classifies images that contain a fovea. Although the script may find some false-positive images in the peripheral retina, it retains only the longest sequence of positive images, thus indicating the true location of the fovea. The central image of this sequence is kept, as it provides the best representation of the central foveal region.

To obtain the coordinates of the fovea relative to the reference area recorded earlier, the script precisely locates the green b-scan line as the y-coordinate through color space conversion, masking, and edge detection techniques, followed by a Hough Line Transform. Since the scan line on the fundus image is a 1:1 match for the adjacent OCT image, the program can gather the x-coordinate of the fovea based on its coordinates in the OCT image. The script first calibrates the X and Y stepper motors via the Telemetrix library by identifying the difference in the fovea's location after moving the stage a set distance.

Subsequently, it moves the motors to position the fovea directly underneath the biopsy punch for sample acquisition.

Sample Handling, Preservation, and *Ex Vivo* Electroretinogram

Trained Utah Lion's Eye Bank technicians recovered human donor eyes, which they immediately submersed in HEPES-buffered Ames's media (Sigma-Aldrich, St. Louis, MO), protected from light, and transferred to the laboratory [15]. In the laboratory, the tissue was processed under dim red-light illumination, and the donor eyes were immediately transferred into bicarbonate-buffered Ames' media, which was oxygenated with 95% O_2 and 5% CO_2. The anterior segment and most of the vitreous was removed, and the retina was imaged using infrared light and OCT (Spectralis, Heidelberg Engineering, MA). To store eyecups or retinal punches attached to the underlying RPE/choroid until *ex vivo* ERG or for long-term incubation to recover light responses following postmortem delay to enucleation, human eyecups and punches were placed in a 150 x 26 mm Petri dish filled with bicarbonate-buffered Ames' media, which was directly bubbled with 95% O_2 and 5% CO_2 inside a Pelican case.

Mice were sacrificed with CO_2 asphyxia followed by cervical dislocation. Eyes were immediately enucleated and dissected by piercing the cornea with a 30 G needle, removing the cornea and iris while leaving the lens in place to ensure we did not disrupt the close interaction between the retina and underlying RPE. We stored mouse eyecups in a 100 mL Pyrex bottle filled with Ames' media, which we either exposed to 95% N_2 and 5% CO_2 to induce hypoxia or oxygenated with 95% O_2 and 5% CO_2.

ERG Recording Protocol

Ex vivo ERG [46] was recorded as described previously [15], [47]. Human or mouse retinas were carefully removed from the underlying RPE/choroid and mounted on the *ex vivo* ERG specimen holder, as described previously. The retinas were superfused with Ames' media containing 100 μM $BaCl_2$ to block K^+ channels on Müller glial cell with or without 40 μM DL-AP4, which blocks signal transmission between photoreceptors and ON-bipolar cells [31], [48]. This allowed the recording of isolated photoreceptor light responses and combined photoreceptor and ON-bipolar cell responses, respectively, and the calculation of isolated ON-bipolar cell responses. We plotted photoreceptor and ON-bipolar cell amplitudes as a function of light flash strengths (photons μm^{-2}) and displayed arithmetic means ± standard error of the mean.

Small-Volume Closed Perfusion System

We built a closed perfusion *ex vivo* electroretinography ERG system that uses a peristaltic pump to circulate small volumes of perfusate. Peripheral retinal pieces from human donor eyes were used with enucleation delays of 1 (UFT8, see Table 1) to 4 (D54_2 and D55, see Table 1) hours. After overnight incubation of the

eyecups, rod photoreceptor responses were recorded at multiple time points over a 12-hour period. The perfusate consisted of HEPES-buffered Ames' media at $32.0 \pm 0.5°C$, an 1-micron pore filter, and Penicillin-Streptomycin (Pen-Strep purchased from Sigma-Aldrich) to prevent bacterial contamination. To isolate the photoreceptor component of the ERG response, 100 μM $BaCl_2$ and 40 μM DL-AP4 were introduced. The dark-adapted retina was stimulated with 505 nm full-field 5 ms flashes. Two dripping burettes were utilized to break the electrical connection and dampen mechanical pulsations from the peristaltic pump. The perfusion system was grounded using Ag/AgCl electrodes (model EP2, World Precision Instruments) through agar gel bridges within the Faraday cage.

Supplementary Data

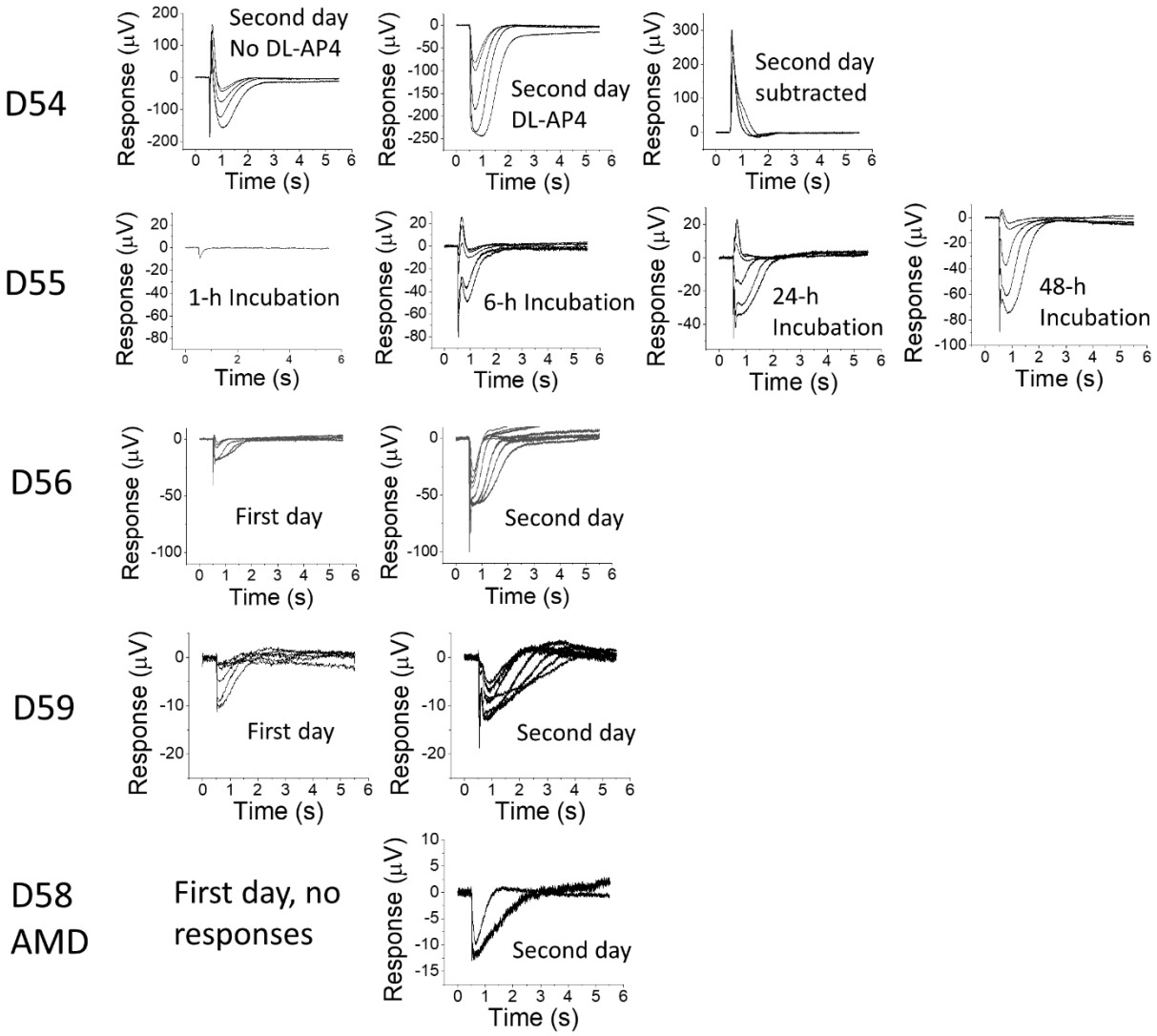

Supplementary Figure 1. Impact of overnight eyecup incubation on the light responses in research donor eyes enucleated 3-4 hours postmortem. Light responses from peripheral retina samples from five research donors (D54, D55, D56, and D58_AMD) from whom eyes were recovered 3-4 hours postmortem (see Table 1 for donor details). D54 and D58_AMD recordings were conducted only after overnight incubation in oxygenated Ames'. Unless indicated otherwise, samples were perfused with Ames' media containing 100 μM Ba^{2+}. For D54, responses are shown in the absence (left) and presence (middle) of 40 μM DL-AP4. The rightmost panel for D54 shows responses derived by subtracting data in the middle panel from that in the left. Light flash strengths (green photons μm^{-2}): D54, 19 – 1,024; D55 (6-h, 24-h and 48-h): 19 – 2,050; D59, First day: 2,300 – 2,500,000, Second day: 19 – 4,100; D56, First day: 57 – 3,900; Second day: 57 – 7,800; D58_AMD: 19 – 16,400.

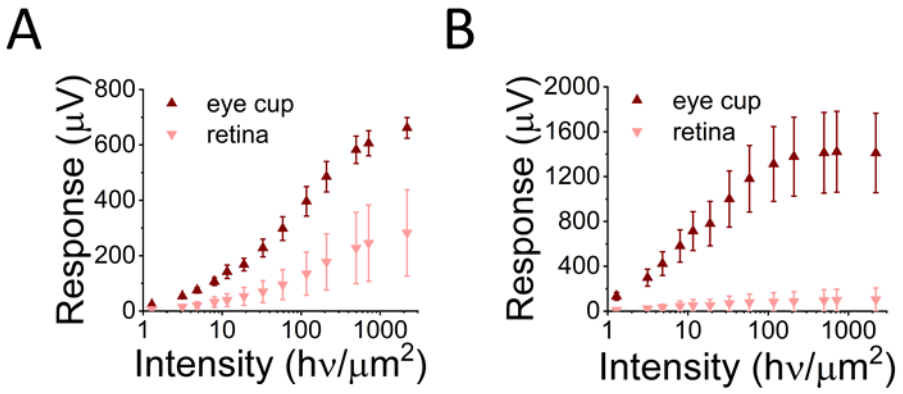

Supplementary Figure 2. RPE dependence of retinal function after overnight storage. (a) *Ex vivo* ON-bipolar and (b) photoreceptor cell light responses after overnight storage of eye cups (n=4) or isolated retinas without underlying RPE (N=3).

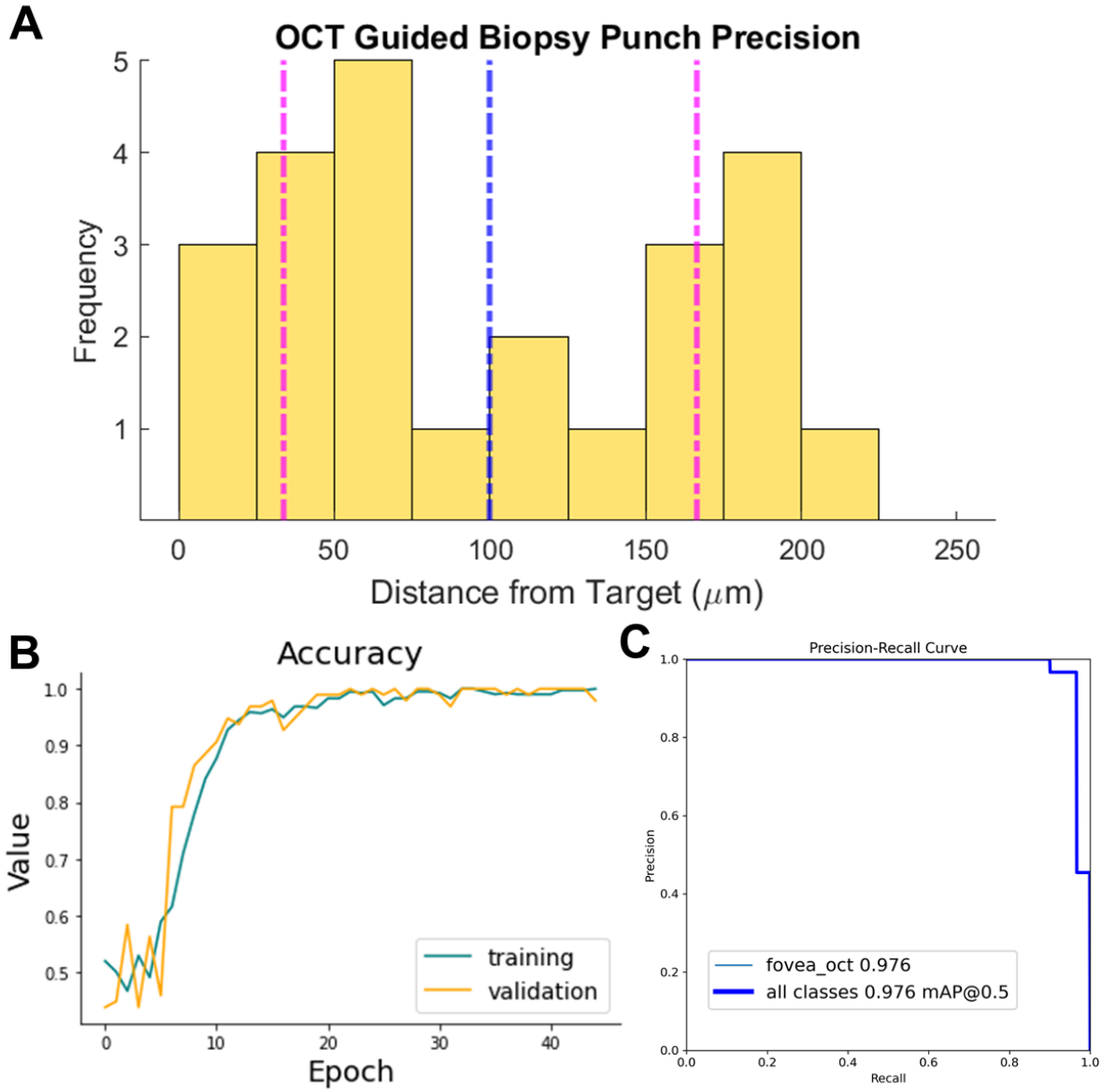

Supplementary Figure 3. OCT and AI model accuracy and precision. (a) Bar chart of OCT precision test displaying the distances between each trial punch (N=24) from the target, with a mean (blue) of 100 ± 66.4 µm (purple). The range of each histogram bin is 25 µm. (b) Accuracy of classification model training on 592 images. The best checkpoint was used for the final model, where accuracy in training and validation was 100%. (c) Precision-Recall curve of object detection model trained on 291 images. The Mean Average Precision at 50% IoU threshold is 97.6%**.**

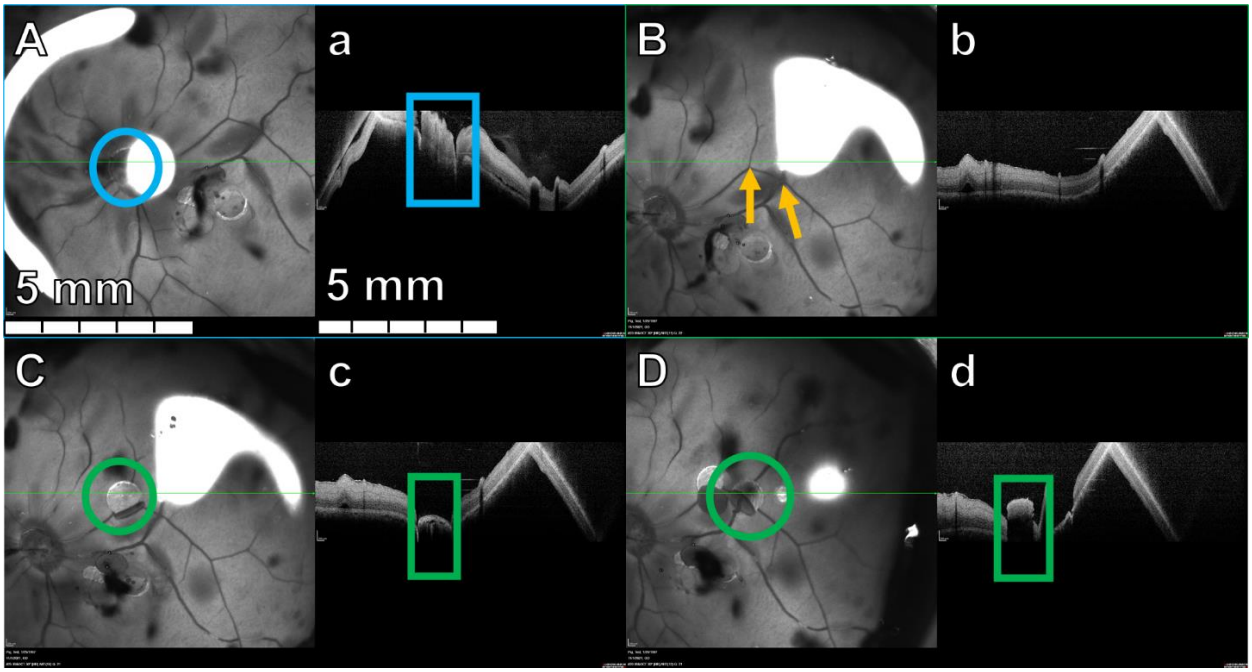

Supplementary Figure 4. Sampling precision in porcine retina. Fundus images (capital letters) are captured with infrared imaging. OCT images (lowercase letters) show cross sectional analysis (relative to b-scan; green line). A reference punch is made (A,a; blue). Two targeted areas are selected (orange arrows in (B)). Biopsy punches are taken (green), (C,c), and (D,d). 100% of targeted areas were successfully sampled (n=9).

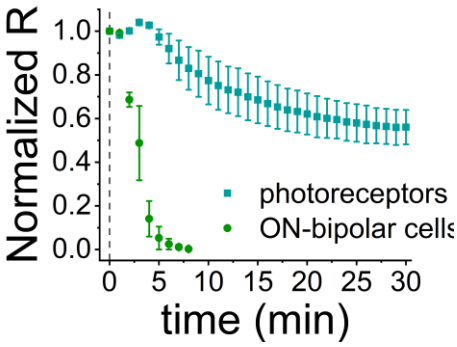

Supplementary Figure 5. Sensitivity of retinal neurons to hypoxia. Photoreceptor (blue) and ON-bipolar cell responses (green) during hypoxia (2.5% O_2), normalized to the response amplitudes before the onset of hypoxia (mean ± SEM, n=3 for photoreceptors, n=2 for ON-bipolar cells).

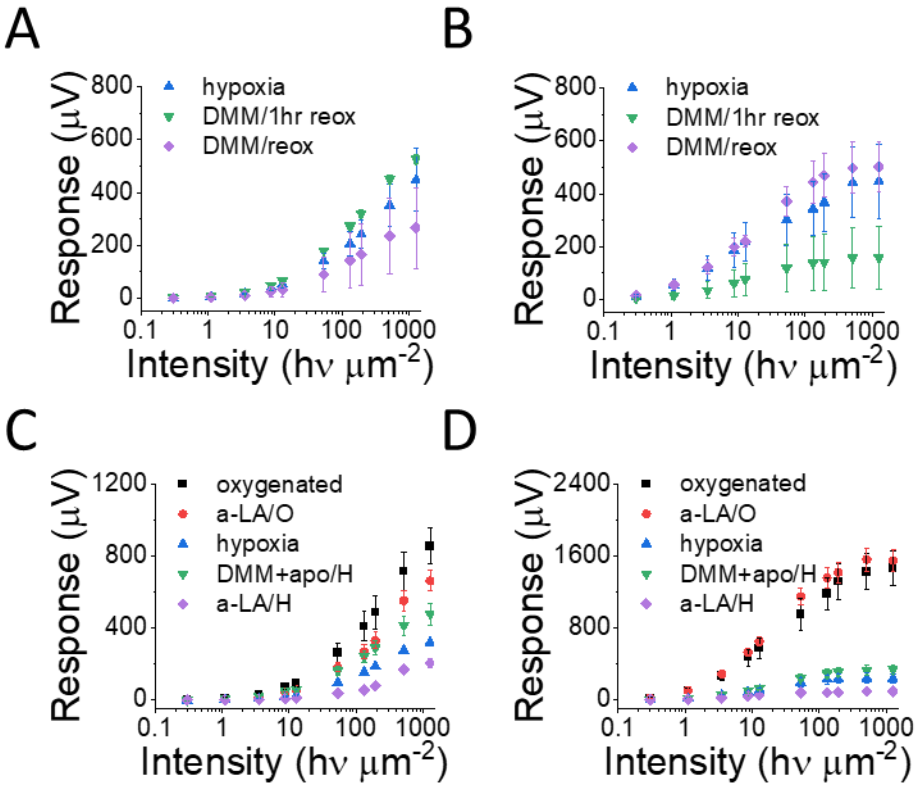

Supplementary Figure 6. Antioxidant drugs during hypoxia and reoxygenation. Photoreceptor (A) and ON-bipolar cell light responses (B) after three hours of hypoxia with overnight incubation in oxygenated Ames' media in the absence or presence of dimethyl malonate (DMM) for 10 min before and one hour during reoxygenation or only during overnight reoxygenation (n=2-3). Photoreceptor (C) and ON-bipolar cell light responses (D) in oxygenated media or after three hours of hypoxia with overnight incubation in oxygenated Ames' media in the absence or presence of α-lipoic acid (a-LA) or DMM+apocynin (DMM+apo, n=4-5).

Supplementary Table 1. Donor information. Preservation delay: Time from cross-clamp (organ donors) or death (research donors) until preservation in Ames' media; SIGSW: self-inflicted gunshot wound; ICB/ICG: intracranial bleeding/hemorrhage; COPD: chronic obstructive pulmonary disease.

Donor ID	Donor type	Preservation delay/mins	Age/sex	Cause of death	Prior medical conditions
UFT2	Organ donor	54	56/male	SIGSW	Type 2 diabetes. no ocular.
UFT3	Organ donor	50	63/female	ICB/ICH	Astigmatism.
UFT6	Organ donor	33	37/female	Respiratory arrest	Asthma, morbid obesity, lactic acid increased. No ocular.
UFT7	Organ donor	22	54/female	ICB/ICH	Cardiomyopathy. No ocular.
UFT8 (Closed perfusion)	Organ donor	68	38/male	Anoxic brain injury	Cardiomyopathy, hypercholesterolemia. Glaucoma.
UFT10	Organ donor	77	57/female	ICB/ICH	Ischemic right carotid artery stroke
D42	Research donor	250	94/male	Pneumonia	Congestive heart failure, diabetes mellitus, diabetic eye disease
D53	Research donor	180	68/female	Cancer	Cardiomyopathy, sepsis
D55	Research donor	247	89/male		
D39 AMD	Research donor	173	90/female		AMD
D46 AMD	Research donor	346	75/male	Surgical complications	AMD, glaucoma
D48 AMD	Research donor	208	89/female	Acute Cardiac Event	
D51 AMD	Research donor	161	96/female	Myocardial infarction	AMD, glaucoma
D57 AMD	Research donor	219	93/female		
D54	Research donor	284	77/female	Cancer	Abnormal EKG, hyperlipidemia, hypertension
D54_2 (Closed perfusion)	Research donor	258	81/Male	Acute Cardiac Event	Chronic venous insufficiency, aortic stenosis, hypoxia, morbid obesity.
D55 (Closed perfusion)	Research donor	249	89/male	Not known	Not known
D59	Research donor	231	78/male	Sepsis	Stroke, lactic acidosis. Vision changes, vision loss.
D56	Research donor	232	82/female	Ischemic bowel	Liver cirrhosis, stroke, COPD, home O2 therapy. Ocular stroke, visual field loss.
D58_AMD	Research donor	219	99/female	Pneumonia	AMD.